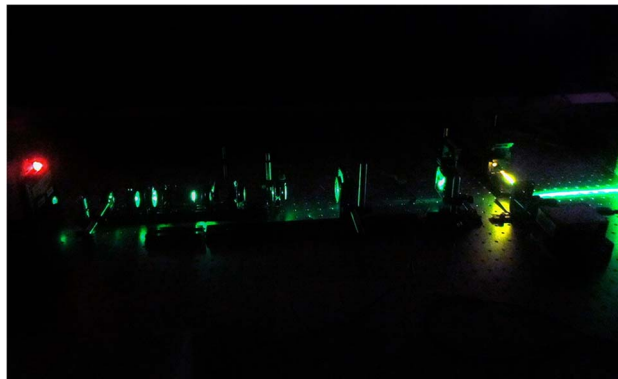


# Laser-Like Performance of Side-Pumped Dye-Doped Polymer Optical Fibers

Volume 7, Number 2, April 2015

J. Arrue  
M. A. Illarramendi  
I. Ayesta  
F. Jiménez  
J. Zubia  
A. Tagaya  
Y. Koike



---

DOI: 10.1109/JPHOT.2015.2406073  
1943-0655 © 2015 IEEE

# Laser-Like Performance of Side-Pumped Dye-Doped Polymer Optical Fibers

J. Arrue,<sup>1</sup> M. A. Illarramendi,<sup>2</sup> I. Ayesta,<sup>3</sup> F. Jiménez,<sup>3</sup>  
J. Zubia,<sup>1</sup> A. Tagaya,<sup>4</sup> and Y. Koike<sup>4</sup>

<sup>1</sup>Department of Communications Engineering, University of the Basque Country (UPV/EHU),  
Escuela Técnica Superior de Ingeniería de Bilbao, 48013 Bilbao, Spain

<sup>2</sup>Department of Applied Physics I, University of the Basque Country (UPV/EHU),  
Escuela Técnica Superior de Ingeniería de Bilbao, 48013 Bilbao, Spain

<sup>3</sup>Department of Applied Mathematics, University of the Basque Country (UPV/EHU),  
Escuela Técnica Superior de Ingeniería de Bilbao, 48013 Bilbao, Spain

<sup>4</sup>Faculty of Science and Technology, Keio University, Yokohama 223-0061, Japan

DOI: 10.1109/JPHOT.2015.2406073

1943-0655 © 2015 IEEE. Translations and content mining are permitted for academic research only.

Personal use is also permitted, but republication/redistribution requires IEEE permission.

See [http://www.ieee.org/publications\\_standards/publications/rights/index.html](http://www.ieee.org/publications_standards/publications/rights/index.html) for more information.

Manuscript received December 15, 2014; revised February 13, 2015; accepted February 18, 2015. Date of publication March 2, 2015; date of current version March 10, 2015. This work was supported in part by the Ministerio de Economía y Competitividad (Spain) under Project TEC2012-37983-C03-01; by the Gobierno Vasco/Eusko Jaurlaritza under Project IT664-13 and Project ETORTEK14/13; by the Fundación Iberdrola under Project FP14/25; by the University of the Basque Country (UPV/EHU) through Program UFI11/16 and Program US13/09; by FEDER funds; and by the Japan Society for the Promotion of Science through the Funding Program for World-Leading Innovative R&D on Science and Technology (FIRST Program), initiated by the Council for Science and Technology Policy. Corresponding author: F. Jiménez (e-mail: felipe.jimenez@ehu.es).

**Abstract:** Mirrorless graded-index polymer optical fibers doped with the organic dye rhodamine 6G result in very compact broadband fiber lasers in the visible region when pumped from the side. The emission spectrum, threshold, and efficiency obtained on both fiber ends depend on the lengths of the directly illuminated region and of the non-excited ones. The paper analyzes such parameters both experimentally and theoretically for the first time.

**Index Terms:** Amplified spontaneous emission, doped polymer optical fibers, organic dyes.

## 1. Introduction

Over the past few decades, the interest in polymer optical fibers (POFs) has steadily increased. On the one hand, they are specially suited for applications in which large diameters or numerical apertures are needed, with the added advantages of allowing operation in the visible region and easy handling. Continuous improvements have been achieved in their attenuation and bandwidth, especially since the development of graded-index (GI) POFs have led to a wide use of them, instead of glass fibers, in short-haul communications links ranging from tens of meters up to lengths of 1 km and exceeding gigabit transmission rates [1]. On the other hand, POFs can also be employed as specific devices for other types of applications, e.g., for the development of sensors [2] or even for the manufacture of active fibers. These include scintillating fibers, fiber lasers, fiber amplifiers and optical switches [3]–[7]. Such devices are based on the light-generation properties of some types of dopants embedded in the POF. For example, organic dyes, in

combination with mirrorless graded-index polymer optical fibers, tend to yield specially compact broadband light sources [6].

In comparison to the performance of conventional fiber lasers based on glass fibers doped with rare earths, there are several advantages or peculiarities in the performance of fiber lasers based on POFs doped with organic dyes. One of them is that the needed POF length can be as short as a few centimeters [8], due to the fact that the optical cross sections of typical organic dyes are about four orders of magnitude larger than those of typical rare earths. Besides, POFs are specially suitable to embed organic dopants in them, in contrast to glass fibers. The reasons for this are the low manufacturing temperatures of POFs and the high ones of glass, and the fact that organic dyes degrade easily with temperature [8]. Another peculiarity is the range of emission wavelengths. Dye-doped POFs serve to obtain visible light of relatively broad spectrum [9], whereas rare earths operate in the infrared and their emission spectra are narrower. In pumped fibers employed as light sources, the phenomenon that takes place is called Amplified Spontaneous Emission (ASE). Although both conventional fiber lasers and mirrorless ones rely on the amplification of stimulated emission, the former ones employ an optical resonator that filters the ASE yielding a narrow emission spectrum, whereas the latter ones do not utilize such a resonator and they simply emit ASE. This is specially suited for some applications. For example, light sources for fiber gyroscopes produce less noise if broad emission spectra are launched into the fiber, e.g., of approximately 20 nm or more [10]. Another interesting characteristic of these active POFs is that their emission can be tuned by changing the fiber length, taking advantage of the significant overlap between the absorption and emission cross sections of some organic dopants. When this overlap is large, it can produce strong shifts in the emission spectra along the fiber. This is the case, for example, of typical rhodamines [11].

Historically, the first fiber laser based on a dye-doped polymer optical fiber was reported in 1987 [12]. Since then, active POFs doped with organic dopants have been studied extensively [13], [18]. One of the materials usually preferred has been rhodamine (B or 6G), which has a very large active area and a strong overlap between its emission and absorption cross sections [6], [11], [19], [20]. POF lasers have been reported both with and without mirrors at the fiber ends. In the latter case, the fiber itself provides enough light confinement to achieve ASE when it is pumped. Specifically, the POF serves to obtain a high power density interacting with the dopant molecules, because light is concentrated in the doped POF core, which increases the probability of stimulated emissions as light travels along the POF up to its output end. As for the type of POF, GI POFs are generally preferable over step-index (SI) ones, because there is a better interaction between light and dopant, owing to the fact that the highest power density is located in the same region as the highest dye concentration, namely in the proximity of the fiber symmetry axis [13]. Therefore, the output energy that can be obtained with GI POFs is greater than that achievable with SI POFs for the same pump energy.

The POF lengths reported are usually shorter than 1 m. High dopant concentrations tend to reduce the fiber lengths necessary to obtain a certain amount of emission power, although there is a limit in the maximum possible concentration of dopant than can be dissolved in the polymer [20]. The optimum fiber length does not only depend on the dopant employed and its concentration but on the pumping characteristics as well. The pump light for a POF working as an amplifier has usually been injected longitudinally at one of the fiber ends. In the case of a POF laser, the pumping scheme can be either longitudinal from one fiber end, or transverse, i.e., from the side [13], [21].

This paper analyzes the parameters affecting ASE emission from side-pumped typical GI POFs made of poly(methyl methacrylate) (PMMA) and doped with rhodamine 6G. As far as we know, this paper is the first one to analyze side-pumped mirrorless POF lasers both theoretically and experimentally. Due to the peculiarities of side pumping, a slightly more complex theoretical model than the one reported by us in a previous paper about longitudinal pumping has had to be employed [13]. The first difference that arises with respect to longitudinal pumping is that the gain volume of the fiber, i.e., the region in which stimulated emissions are dominant over absorptions, can be extended for longer distances [22]. This paper illustrates the consequences of

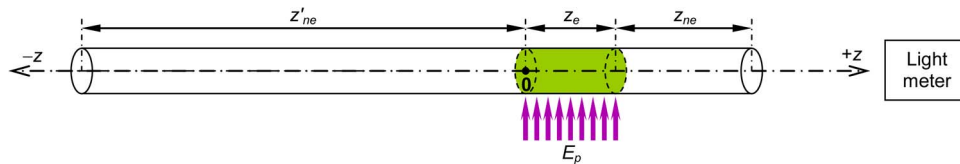


Fig. 1. Side-pumping scheme in which a region  $z_e$  is illuminated transversely from the side, which, in turn, produces light at new wavelengths that propagate both in the  $+z$  direction, i.e., toward the light meter, and in the  $-z$  direction.  $z_{ne}$  is the non-excited length closest to the light meter.  $z'_{ne}$  is the left-side non-excited length.

this fact both with experimental and with computational results. First of all, in Section 2, we describe the experimental set-up. In Section 3, we describe the way to computationally calculate the absorbed pump power and to treat its effects, which is different with both pumping techniques (longitudinal and transverse). Specifically, now we consider propagation in both senses along the fiber, which allows us to quantify the effect, on one of the fiber ends, of the fraction of the energy propagating toward the opposite fiber end that eventually returns backward. In Section 4, we analyze the most general case of employing asymmetrical illumination, i.e., of pumping closer to one of the ends than to the other. The parameters analyzed are the excited length, i.e., the one directly illuminated, and the non-excited lengths on the right and on the left of it. The study focuses on the influence of these lengths on the ASE spectrum, threshold, and efficiency obtained for each one of the fiber ends when side pumping is utilized.

## 2. Experimental Setup

The fiber analyzed is a GI POF whose core is doped with rhodamine 6G at a concentration of 12 ppm in weight and whose cladding is not doped. The core diameter is 0.6 mm, and the total fiber diameter including the cladding is 1 mm. Since the fiber considered is a GI one, the interaction between light and dopant is overall stronger than in the case of the uniform radial distributions of light and dopant that are typical of step-index fibers. This effect is taken into account by means of an overlapping factor  $\gamma$ , which was determined from experimental measurements [13]. This factor  $\gamma$  is typically between 1 and 2 in GI fibers, the higher values corresponding to stronger interactions. For our GI fiber, we obtained  $\gamma = 1.7$  [9].

For the measurements, the fiber was cut into samples of various lengths (20–30 cm), and the fiber ends were carefully polished by hand with polishing papers. In all measurements, the fiber was pumped from the side by focusing the light onto the fiber as a stripe of 1 mm in height whose horizontal length  $z_e$  could be changed by means of a set of three lenses. Further details on the characteristics and alignment of these fibers and of the lenses employed can be found in [23]. As pump source, we employed the frequency-doubled output (532 nm) of a 10 Hz Q-switched Nd:YAG laser. This emitted approximately Gaussian pulses whose temporal full width at half maximum was about 20 ns. The pulse energy was controlled by insertion of calibrated neutral density filters into the beam path. To measure the emission spectra of the side-pumped POF, we employed a fiber-optic spectrometer (USB4000) with an optical resolution of 1.5 nm of full width at half maximum. All the emission spectra were corrected for the response of the detection system.

## 3. Theoretical Model

Our model considers the light power propagating along the fiber in its positive direction ( $+z$ ), and also the one propagating in its negative direction ( $-z$ ), as functions of three independent variables, namely  $z$  (position along the fiber axis),  $t$  (time) and  $\lambda$  (light wavelength). We call these  $P^+(t, z, \lambda)$  and  $P^-(t, z, \lambda)$ , respectively. The geometry is illustrated in Fig. 1.

The model also considers two energy states to describe the dopant embedded in the fiber: a ground energy state 1, and an excited state 2. This is a reasonable simplification for active POFs doped with organic dopants, as is the case of rhodamine 6G [6]. There are  $N_1(t, z)$  and

$N_2(t, z)$  molecules per unit volume in each state, respectively. The total concentration of dopant  $N$  is constant along  $z$ , so  $N_1(t, z) + N_2(t, z) = N$ . The evolutions of  $P^+(t, z, \lambda)$ ,  $P^-(t, z, \lambda)$  and  $N_2(t, z)$  are governed by a set of partial differential equations called the rate equations [6], which we have adapted for the double sense of propagation in the way that will be explained below.

We launch a temporal pulse of total pump energy  $E_p$  at wavelength  $\lambda_p$ . The absorbed energy serves to increase  $N_2$  in the illuminated region. This increase in  $N_2$ , i.e., the number of transitions from state 1 to state 2 per unit volume, depends on the fraction of  $E_p$  that is absorbed. Since the pumping is from the side, a relatively large fraction of the pump energy can cross unabsorbed to the other side of the fiber, because the path of light through the doped region is short. In order to calculate the fraction of pump absorbed, we have assumed that there is an average distance  $d_{av}$  travelled by the side-pumped rays through the doped region of the fiber across a depth that is approximately equal to the fiber core diameter. It would be theoretically possible to use the ray tracing method, taking into account the multiple reflections of pumped light rays at the internal surface of the fiber, but this can be very complex. The fraction of energy absorbed at each time is therefore approximated as  $1 - \exp(-\alpha d_{av})$ , where the attenuation coefficient  $\alpha$  is calculated as  $\alpha = N_1(t, z) \cdot \sigma^a(\lambda_p)$ . Dividing the energy absorbed by the energy necessary to excite one molecule we obtain the number of molecules that are excited during a small time interval  $\delta t$ , and dividing this number by the pumped volume we get the corresponding increment in  $N_2$ . The effect of  $P^\pm$  on  $N_2$  inside the pumped region will also be taken into account. In turn, the population  $N_2$  obtained in these ways can decay, with both spontaneous and stimulated emissions, generating power both in the  $+z$  and in the  $-z$  directions, namely  $P^+$  and  $P^-$ . Only one of the fiber ends is employed as output (see Fig. 1). The introduction of back propagation in the model allows us to quantify not only the effect of the directly excited segment  $z_e$ , but also the influence of the non-excited fiber lengths  $z_{ne}$  and  $z'_{ne}$ ,  $z_{ne}$  being the one closest to the light meter.

The dependence of the light power on wavelength is introduced by means of the emission and absorption cross sections of the dopant. For each wavelength  $\lambda$ , the evolutions of  $P^+(t, z, \lambda)$ ,  $P^-(t, z, \lambda)$  and  $N_2(t, z)$  are governed by two rate equations. One of them governs the change of the excited population density  $N_2$  with time, as follows:

$$\frac{\partial N_2(t, z)}{\partial t} = \int_0^\infty \frac{P^+(t, z, \lambda) + P^-(t, z, \lambda)}{hf} \gamma [\sigma^a(\lambda) \cdot (N - N_2(t, z)) - \sigma^e(\lambda) \cdot N_2(t, z)] d\lambda - \frac{N_2(t, z)}{\tau}$$

where  $h$  is Planck's constant;  $f = c/\lambda$  is the light frequency,  $c$  being the speed of light in vacuum;  $\sigma^a(\lambda)$  and  $\sigma^e(\lambda)$  are the absorption and emission cross sections of the dopant;  $\tau$  is the spontaneous lifetime of the dopant in the excited state; and  $\gamma$  is the aforementioned factor that takes into account the amount of overlap between the radial distributions of light power and dopant concentration.

A second rate equation governs the light power  $P^\pm$  propagating in both directions:

$$\frac{\partial P^\pm}{\pm \partial z} = \sigma^e(\lambda) N_2 P^\pm \gamma - \sigma^a(\lambda) N_1 P^\pm \gamma - \frac{1}{c/n} \frac{\partial P^\pm}{\partial t} + \frac{N_2}{\tau} \left( \frac{h c}{\lambda} \right) \sigma_{sp}^e(\lambda) \beta A_{core}$$

where  $n$  is the maximum core refractive index;  $\beta$  is the average value, in our GI fiber, of the fraction of spontaneous emissions that are guided along the fiber, and it was calculated in [9] for the same doped fiber; and  $\sigma_{sp}^e(\lambda)$  is the spontaneous emission cross section, i.e., the probability distribution of the wavelengths of spontaneously emitted photons.

In our case, the initial conditions for those equations are, simply, that at  $t = 0$  there is no light power propagating in the fiber and no excited population, i.e.,  $P^+(0, z, \lambda) = 0$ ,  $P^-(0, z, \lambda) = 0$ ,  $N_2(0, z) = 0$ . The values of  $N_2$  in the pumped region, i.e., in  $z_e$ , are incremented as explained above to take the external pump into account.

To solve these equations numerically we have written an ad-hoc finite-difference-based computer program that discretizes all three independent variables  $t, z, \lambda$  [9]. The program simulates

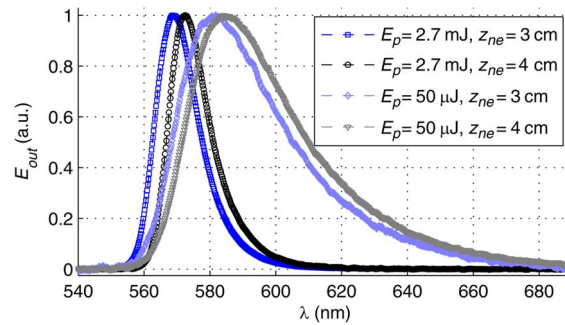


Fig. 2. Experimental normalized emission spectra obtained at the output end of the fiber when  $z_{ne}$  is 3 and 4 cm for two pumping energies, which are below and above threshold, respectively.  $z_{ne} = 2$  cm in all cases.

the evolution of the system in discrete time increments  $\delta t$ . The wavelength dependence is introduced by dividing the spectrum into discrete intervals of  $\lambda$  centered at wavelengths  $\lambda_k$  and taking into account the spectral curves of the absorption and emission cross sections of the dopant [11]. The cross sections for absorption and emission of the analyzed material were measured by some of the authors [16]. These measurements were previously performed in doped PMMA bulk. The spectral shapes of the cross sections in our own fiber were determined from the absorption and emission spectra measured in a short segment of fiber, and we used the peak values of the curves determined in bulk to obtain the absolute values of the cross sections in our fiber.

## 4. Results and Discussion

### 4.1. Influence of the Non Excited Length Adjacent to the Light Meter

Let us firstly analyze the influence of  $z_{ne}$  (see Fig. 1). To obtain the corresponding results, we maintained the transversely illuminated length  $z_e = 2$  cm for all values of  $z_{ne}$ , and we employed a sufficiently long fiber section  $z'_{ne}$  on the opposite side of the light meter to ensure that further lengthening of  $z'_{ne}$  would not have had any significant effect on the measured or calculated power. Specifically,  $z'_{ne}$  was approximately equal to 18 cm in all cases. From a theoretical point of view, this distance is long enough to reduce the new emissions to insignificant values at the farthest end in the  $-z$  direction, because  $N_2$  tends to become negligible due to the great attenuation of the light power along  $z'_{ne}$ . On the side of the light meter, the minimum value of  $z_{ne}$  was limited by the fact that the fiber had a connector at its end in the experimental set-up, so we could only vary  $z_{ne}$  from a minimum distance on the order of 3 cm. By increasing  $z_{ne}$  in small steps we examine the influence of this parameter on the output light spectrum, the threshold energy and the efficiency. The experimental emission spectra obtained at the output end of the fiber for two values of  $z_{ne}$  are illustrated in Fig. 2 when the pump energy is above and below the threshold value. We notice that the spectral curves above threshold (ASE emission) are not only much narrower, as expected, but they are also blue-shifted toward the peak wavelength of the emission cross section of the dopant, as was explained by us in [11]. As can be seen, the curve for  $z_{ne} = 4$  cm for the case below threshold ( $E_p = 50 \mu\text{J}$ ) is red-shifted with respect to the curve for  $z_{ne} = 3$  cm: the average wavelength is  $\lambda_{av} = 595$  nm for  $z_{ne} = 3$  cm and  $\lambda_{av} = 601$  nm for  $z_{ne} = 4$  cm. The corresponding peak wavelengths are 581 nm and 585 nm, respectively. These shifts are due to the overlap between the emission and absorption cross sections and to the light propagation distance along the fiber [11].

Regarding the evolution of the output spectrum width (full width at half maximum, or FWHM), Fig. 3(a) shows that the theoretically and experimentally obtained spectra narrow abruptly when the pump energy is increased above a certain value. This behavior has been used by some researchers to define the ASE threshold as the pump energy necessary for the FWHM of the

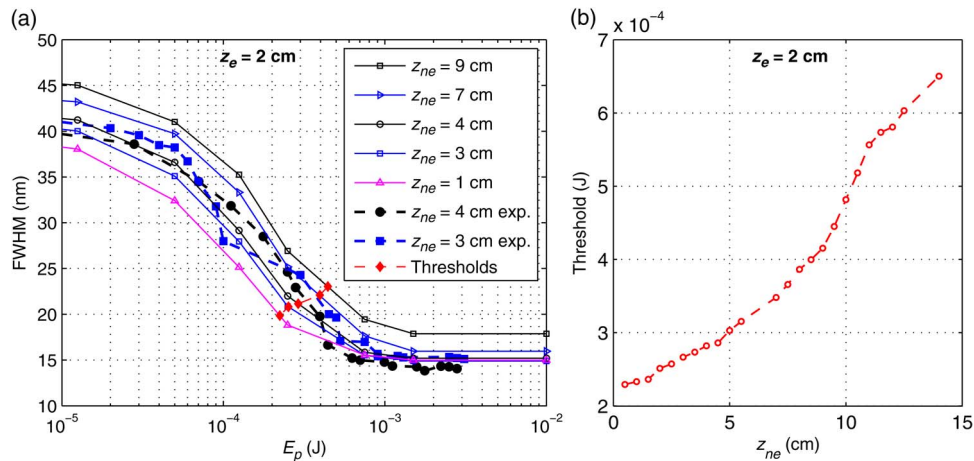


Fig. 3. (a) Dependence of the spectral FWHM of the output emission on the pump energy for transverse excitation of a length  $z_e = 2$  cm for various values of the right-side non-excited length  $z_{ne}$ . Solid lines: computational curves, with the corresponding threshold points. Dashed lines join experimental points. (b) Computationally calculated threshold energy as a function of  $z_{ne}$ .

emitted intensity to drop to half the value observed when the sample is pumped with low energy [17]. With this criterion, we have marked the points of 50% spectral width reduction in each of the theoretical curves of Fig. 3(a), which indicate the corresponding threshold energies. These points have been calculated from the sigmoid curve that best fits the points of each curve of Fig. 3(a). We can observe that these thresholds tend to shift toward higher values when  $z_{ne}$  is increased, which can be explained if we take into account that the values of  $N_2$  are much lower in  $z_{ne}$  than in the pumped length  $z_e$ , especially at points located far enough from  $z_e$ . Therefore, higher pump energies are needed to compensate for the extra losses of a longer  $z_{ne}$  in order to obtain net amplification over the entire fiber length. This net amplification is what narrows the ASE spectrum, since wavelengths in the proximity of the emission peak wavelength are more amplified than the others. The dashed lines are joining experimental points for two values of  $z_{ne}$  inside the same range of lengths considered. Both in the theoretical and in the experimental results, the thresholds are also located in the same range of energies. Fig. 3(b) shows the threshold energy as a function of  $z_{ne}$ , calculated computationally. We can see that this increase occurs more rapidly when  $z_{ne}$  takes intermediate values rather than very small ones, which can be explained from the small but still significant presence of excited molecules in the proximity of the illuminated region, thus reducing attenuation. Very far away, the slope of the curve reduces again due to the absence of changes in attenuation. In other words, the most rapid changes in attenuation coincide with the most rapid changes in threshold.

The dependence of the ASE efficiency on  $z_{ne}$  has been calculated computationally and plotted in Fig. 4. It is calculated as follows. By plotting the evolution of the total output energy, i.e., the energy integrated over all emitted wavelengths, as we increase the pump energy from  $1 \mu\text{J}$  to a maximum of  $3 \text{ mJ}$  for each value of  $z_{ne}$  considered, we calculate the corresponding slope of the curve in the region in which this is steepest and approximately linear. The slope of the curve tends to increase rather suddenly to a constant high value in the proximity of the ASE threshold. Such slope can be called slope efficiency or, simply, efficiency. From Figs. 3(b) and 4, we can see that both the threshold and the efficiency tend to worsen with fiber length, i.e., with  $z_{ne}$ , for a constant  $z_e$ . This fact can be explained by taking into account that the non-excited segment  $z_{ne}$  clearly extends outside the gain volume of the fiber, which is, basically, the region of  $z_e$ . Therefore, as can also be seen in Fig. 4, attenuation dominates clearly in  $z_{ne}$ , in which the efficiency decays in an approximately exponential fashion at points that are sufficiently separated from the pumped volume. Specifically, it takes the same shape as that of the emitted light power, as was justified in [13]. In other words, the curve of the efficiency is approximately proportional to

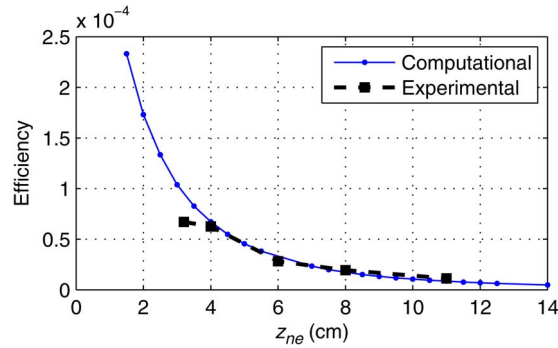


Fig. 4. ASE efficiency as a function of the right-side non-excited fiber length  $z_{ne}$ . Solid lines: computational curves. Dotted line joins experimental points.

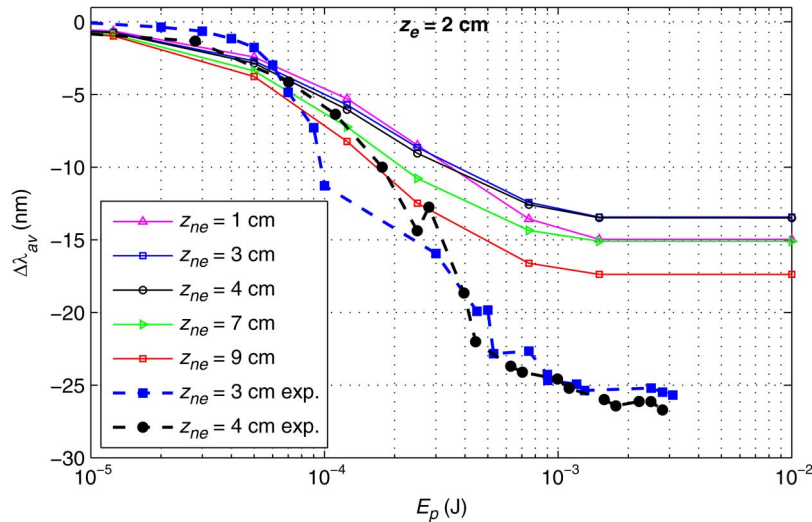


Fig. 5. Dependence of the average wavelength of the output emission on the pump energy for transverse excitation of a length  $z_e = 2$  cm for various values of the right-side non-excited length  $z_{ne}$ . The curves show the relative shift of the average wavelength of the output emission with respect to the initial wavelength (approximately  $600 \pm 15$  nm, depending on  $z_{ne}$ ). Solid lines: computational curves. Dashed lines join experimental points.

$\exp(-\alpha z_{ne})$ , where  $\alpha$  is the net attenuation coefficient of the fiber corresponding to all emitted wavelengths, provided that  $z_{ne}$  is large enough. In Fig. 4, we can also see the experimental efficiencies (dotted line) and their tendency to decrease with the same slope as the theoretical curve. In the experimental curve, the minimum value of  $z_{ne}$  is 3 cm because of the space constraints of the connector commented above. Since the experimental efficiencies obtained are in arbitrary units, the experimental curve in Fig. 4 has been normalized according to the computational one, in order to show the coincidence of slopes.

Fig. 5 shows that, as the pump energy is increased above the threshold energy, there is a shift in the output toward shorter average wavelengths (negative increment  $\Delta\lambda_{av}$ ), i.e., toward the peak of the emission cross section. This effect is a consequence of the strong overlap between the absorption and emission processes that take place along the doped fiber [11], [20]. The same tendency is corroborated both by computational results (solid lines) and by experimental ones (dashed lines). The influence of  $z_{ne}$  on the shift is small, as compared to that of the pump energy, because most of the stimulated emissions, which are the ones causing the spectral shift, occur in  $z_e$ , where  $N_2$  is much greater than in  $z_{ne}$ . The experimentally obtained shifts are larger than the theoretical ones, as if  $E_p$  caused a greater effect than that expected



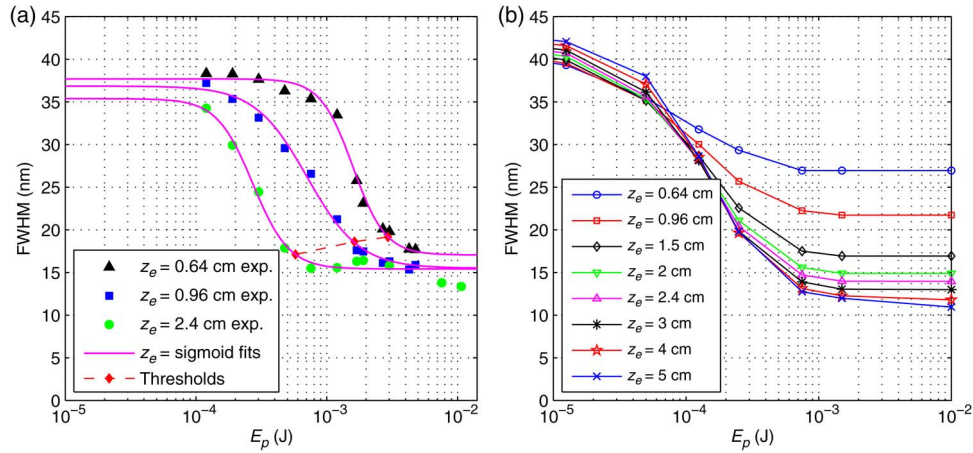


Fig. 6. Dependence of the spectral FWHM of the output emission on the pump energy for various lengths of the excited region  $z_e$ , maintaining  $z_{ne} = 3.2$  cm for all cases, both in the experimental curves (a) and in the computational ones (b).

theoretically. This might be due to the fact that our model assumes that the only direct effect of the fraction of  $E_p$  absorbed in the side-pumped volume is to increase the population  $N_2$ , neglecting the small fraction of pump light that could be scattered in almost-perpendicular directions that can be guided, or the extra fraction absorbed due to internal reflections. Both effects would make a larger fraction of  $E_p$  to be absorbed than the one corresponding to an average distance  $d_{av}$  equal to the fiber core diameter (see Section 3).

#### 4.2. Influence of the Excited Length

In Fig. 6, we show the evolution of the FWHM of the emission spectrum as a function of the pump energy obtained experimentally (a) and computationally (b), for various excited lengths  $z_e$ . Fig. 6(a) also includes the sigmoid functions that best fit the experimental points in order to calculate the threshold points as the points of 50% FWHM reduction. We can see that the thresholds decrease as  $z_e$  increases, because a greater gain volume tends to augment the possibility of stimulated emissions and, thus, to reduce threshold. Besides, if  $z_e$  increases, a greater fraction of  $E_p$  can be absorbed because  $N_1$  increases, which also tends to reduce the threshold energy. However, if  $z_e$  became too large, there would be an excessive reduction in the absorbed pump intensity, since it would be spread in a very large volume. As a consequence, we can expect that the benefits of a larger gain volume would be cancelled out by this spread of the absorbed pump, so threshold points would no longer shift to smaller energies provided that  $z_e$  were increased too much. Fig. 6(b) confirms this expected behavior for the largest values of  $z_e$ , i.e., 3, 4 or 5 cm, since the curves do not show significant further reduction in the FWHM as  $z_e$  is increased.

Fig. 7(a) illustrates the theoretical dependence of the threshold on the illuminated length  $z_e$ , showing clearly that there is a value of  $z_e$  for which the threshold is minimum. To explain this behavior, in Fig. 7(b), we have plotted the theoretical absorbed light intensity as a function of  $E_p$  and  $z_e$ . This intensity is proportional to the absorbed pump energy divided by  $z_e$ , which has a maximum and then it decreases as  $z_e$  increases. This maximum intensity can explain the already commented minimum in Fig. 7(a). The minimum threshold and the maximum absorbed intensity occur around the same values of  $z_e$  (5 cm in our case).

As can be expected, increasing  $z_e$  does not only affect the spectral width of the output, but it also changes its average wavelength. Fig. 8(a) shows that there is a negative shift in the experimentally obtained  $\lambda_{av}$ , i.e., toward shorter wavelengths, as  $z_e$  is increased with moderate or small values of  $z_e$ . This happens because the length of the gain volume is increased, so stimulated emissions become more important and the spectrum shifts toward the peak wavelength of

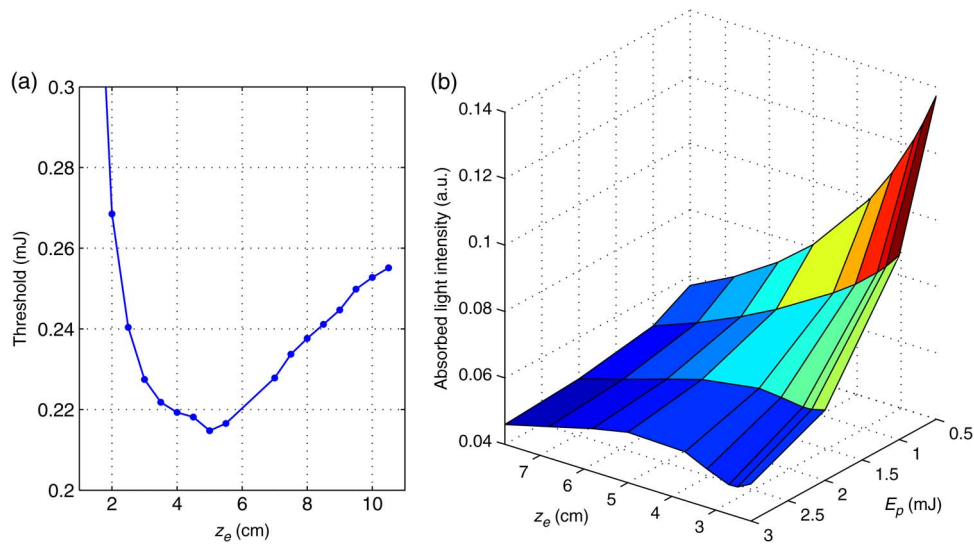


Fig. 7. (a) Dependence on the illuminated length  $z_e$  of the thresholds calculated from the pump energies that yield a 50% reduction in spectral width with respect to the width for low energies. (b) Absorbed energy density, i.e., absorbed energy divided by  $z_e$ , as a function of both  $z_e$  and the pump energy.

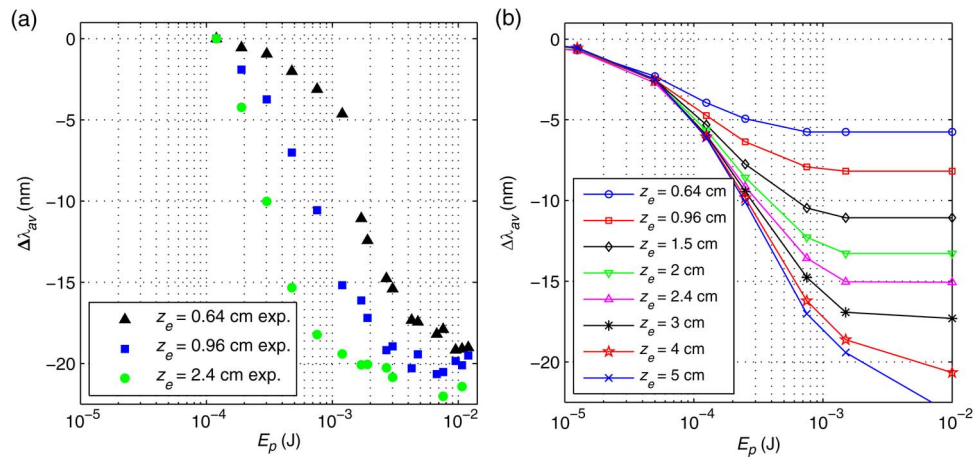


Fig. 8. Dependence on the pump energy of the shift in the average wavelength of the output emission for various lengths of the excited region  $z_e$ , maintaining  $z_{ne} = 3.2$  cm for all cases, both in the experimental curves (a) and in the computational ones (b).

the emission cross section. The figure corresponds to experimental points, for which the maximum length  $z_e$  that could be illuminated was 2.4 cm. For a larger range of values of  $z_e$ , we have calculated the shifts computationally. The results are shown in Fig. 8(b), which confirms the expected saturation effect in the shift of the average wavelength when  $z_e$  becomes very large that was commented in Fig. 6(b) for the FWHM. The discrepancies between the theoretical and the experimental curves plotted in Figs. 6 and 8 could be due to the phenomena that are not contemplated in our computational model, such as the scattering of the pump in guided directions or the multiple reflections of some of the pumped rays.

In all the previous simulations, the length  $z'_{ne}$  on the side located opposite to the light meter was maintained constant and equal to 18 cm, since further lengthening of this side has no effect on the end of the light meter. However, if  $z'_{ne}$  is reduced sufficiently, there can be fewer opportunities for emissions inside it, which would also affect the output energy. This effect can be

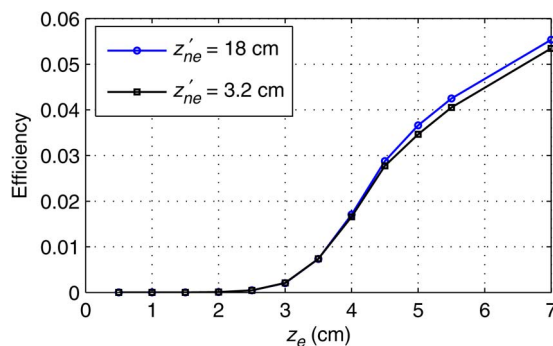


Fig. 9. ASE efficiency as a function of the illuminated length  $z_e$ , both with 18 cm and with 3.2 cm of non-illuminated fiber on the side opposite from the light meter.

detected computationally thanks to the propagation in both senses being considered. Fig. 9 shows that the influence of  $z'_{ne}$  is small, with slightly greater efficiencies when we increase  $z'_{ne}$ . This effect is more noticeable when the illuminated area  $z_e$  is longer. In any case, the tendency is for the efficiency to increase with the excited length  $z_e$ , although this increase occurs more slowly when  $z_e$  is large enough, because of the already commented reduction in the absorbed pump intensity.

## 5. Conclusion

We have carried out a detailed study of the mirrorless ASE emission in a rhodamine-6G doped graded-index polymer optical fiber pumped transversely. We have shown how the output ASE is affected by the length of the directly-excited volume and by the lengths of the non-excited segments of fiber at both sides of the excited length. Effects such as spectral narrowings and shifts of the emission average wavelength have been analyzed both experimentally and computationally when varying the aforementioned parameters. We have also shown that a theoretical model based on the rate equations can serve to successfully predict the laser-like emission features in side-pumped fibers. The dependence on fiber length of the theoretical thresholds and efficiencies for all emission wavelengths has been analyzed as well. The results indicate that there is a certain value of the excited length for which the threshold is minimum and also that the efficiency tends to increase as the excited length is increased, although the efficiency tends to saturate when the excited length becomes too large. The non-excited length on the opposite side of the light meter has been shown to have little influence on the output.

## References

- [1] T. Ishigure, S. Tanaka, E. Kobayashi, and Y. Koike, "Accurate refractive index profiling in a graded-index plastic optical fiber exceeding gigabit transmission rates," *J. Lightw. Technol.*, vol. 20, no. 8, pp. 1449–1456, Aug. 2002.
- [2] P. Aiestaran, J. Arrue, and J. Zubia, "Design of a sensor based on plastic optical fibre (POF) to measure fluid flow and turbidity," *Sensors*, vol. 9, no. 5, pp. 3790–3800, May 2009.
- [3] I. Ayesta *et al.*, "Luminescence study of polymer optical fibers doped with conjugated polymers," *J. Lightw. Technol.*, vol. 30, no. 21, pp. 3367–3375, Nov. 2012.
- [4] J. Zubia and J. Arrue, "Plastic optical fibers: An introduction to their technological processes and applications," *Opt. Fiber Technol., Mater., Devices Syst.*, vol. 7, no. 2, pp. 101–140, 2001.
- [5] M. G. Kuzyk, *Polymer Fiber Optics: Materials, Physics, and Applications*. Boca Raton, FL, USA: CRC, 2007.
- [6] J. Arrue, F. Jiménez, I. Ayesta, M. Asuncion Illarramendi, and J. Zubia, "Polymer-optical-fiber lasers and amplifiers doped with organic dyes," *Polymers*, vol. 3, no. 3, pp. 1162–1180, Jul. 2011.
- [7] A. Charas *et al.*, "Gain and ultrafast optical switching in PMMA optical fibers and films doped with luminescent conjugated polymers and oligomers," *Frontiers Optoelectron. China*, vol. 3, no. 1, pp. 45–53, 2010.
- [8] A. Tagaya, S. Teramoto, E. Nihei, K. Sasaki, and Y. Koike, "High-power and high-gain organic dye-doped polymer optical fiber amplifiers: Novel techniques for preparation and spectral investigation," *Appl. Opt.*, vol. 36, no. 3, pp. 572–578, Jan. 1997.
- [9] I. Ayesta, J. Arrue, F. Jiménez, M. A. Illarramendi, and J. Zubia, "Analysis of the emission features in graded-index polymer optical fiber amplifiers," *J. Lightw. Technol.*, vol. 29, no. 17, pp. 2629–2635, Sep. 2011.

- [10] M. J. F. Digonnet, *Rare Earth Doped Fiber Lasers and Amplifiers*. New York, NY, USA: Marcel Dekker, 1993.
- [11] J. Arrue *et al.*, "Computational analysis of the power spectral shifts and widths along dye-doped polymer optical fibers," *Proc. Inst. Elect. Eng.—Photon. J.*, vol. 2, no. 3, pp. 521–531, Jun. 2010.
- [12] S. Muto, A. Ando, O. Yoda, T. Hanawa, and H. Ito, "Dye laser by sheet of plastic fibers with wide tuning range," *Trans. IEICE Japan*, vol. E70, no. 4, pp. 317–318, 1987.
- [13] M. A. Illarramendi *et al.*, "Amplified spontaneous emission in graded-index polymer optical fibers: Theory and experiment," *Opt. Exp.*, vol. 21, no. 20, pp. 24 254–24 266, Oct. 2013.
- [14] D. Amarasinghe, A. Ruseckas, G. A. Turnbull, and I. D. W. Samuel, "Organic semiconductor optical amplifiers," *Proc. IEEE*, vol. 97, no. 9, pp. 1637–1650, Sep. 2009.
- [15] J. Clark *et al.*, "Blue polymer optical fiber amplifiers based on conjugated fluorene oligomers," *J. Nanophoton.*, vol. 2, no. 1, 2008, Art. ID. 023504.
- [16] A. Tagaya *et al.*, "Theoretical and experimental investigation of rhodamine B-doped polymer optical fiber amplifiers," *IEEE J. Quantum Electron.*, vol. 31, no. 12, pp. 2215–2220, Dec. 1995.
- [17] R. Xia, G. Heliotis, Y. Hou, and D. D. C. Bradley, "Fluorene-based conjugated polymer optical gain media," *Organic Electron.*, vol. 4, no. 2–3, pp. 165–177, Sep. 2003.
- [18] L. Bazzana *et al.*, "Plastic optical fibers with embedded organic semiconductors for signal amplification," in *Proc. 16th Int. Conf. Plastic Opt. Fibers*, 2001, pp. 327–332.
- [19] J. Clark and G. Lanzani, "Organic photonics for communications," *Nature Photon.* vol. 4, no. 7, pp. 438–446, 2010.
- [20] E. De la Rosa-Cruz, C. W. Dirk, A. Rodríguez, and V. M. Castaño, "Characterization of fluorescence induced by side illumination of rhodamine B doped plastic optical fibers," *Fiber Integr. Opt.*, vol. 20, no. 5, pp. 457–464, 2001.
- [21] K. Kuriki *et al.*, "High-efficiency organic dye-doped polymer optical fiber lasers," *Appl. Phys. Lett.*, vol. 77, no. 3, pp. 331–333, Jul. 2000.
- [22] R. Kruhlak and M. Kuzy, "Side-illumination fluorescence spectroscopy. I. Principles," *JOSA B*, vol. 16, no. 10, pp. 1749–1755, Oct. 1999.
- [23] M. A. Illarramendi *et al.*, "Longitudinal versus transversal excitation in doped graded-index polymer optical fibers," *Proc. SPIE*, vol. 8983, pp. 89830G1–89830G7, Mar. 2014.